

## Base-Induced Decomposition of Alkyl Hydroperoxides in the Gas Phase. Part 3. Kinetics and Dynamics in $\text{HO}^- + \text{CH}_3\text{OOH}$ , $\text{C}_2\text{H}_5\text{OOH}$ , and *tert*- $\text{C}_4\text{H}_9\text{OOH}$ Reactions<sup>†</sup>

Shuji Kato,<sup>\*,‡</sup> G. Barney Ellison,<sup>‡</sup> Veronica M. Bierbaum,<sup>‡</sup> and Stephen J. Blanksby<sup>\*,§</sup>

Department of Chemistry and Biochemistry, University of Colorado and JILA, University of Colorado and National Institute of Standards and Technology, Boulder, CO 80309, and School of Chemistry, University of Wollongong, NSW 2522, Australia

Received: January 24, 2008; Revised Manuscript Received: April 15, 2008

The  $\text{E}_{\text{CO}2}$  elimination reactions of alkyl hydroperoxides proceed via abstraction of an  $\alpha$ -hydrogen by a base:  $\text{X}^- + \text{R}^1\text{R}^2\text{HCOOH} \rightarrow \text{HX} + \text{R}^1\text{R}^2\text{C}=\text{O} + \text{HO}^-$ . Efficiencies and product distributions for the reactions of the hydroxide anion with methyl, ethyl, and *tert*-butyl hydroperoxides are studied in the gas phase. On the basis of experiments using three isotopic analogues,  $\text{HO}^- + \text{CH}_3\text{OOH}$ ,  $\text{HO}^- + \text{CD}_3\text{OOH}$ , and  $\text{H}^{18}\text{O}^- + \text{CH}_3\text{OOH}$ , the overall intrinsic reaction efficiency is determined to be 80% or greater. The  $\text{E}_{\text{CO}2}$  decomposition is facile for these methylperoxide reactions, and predominates over competing proton transfer at the hydroperoxide moiety. The  $\text{CH}_3\text{CH}_2\text{OOH}$  reaction displays a similar  $\text{E}_{\text{CO}2}$  reactivity, whereas proton transfer and the formation of  $\text{HOO}^-$  are the exclusive pathways observed for  $(\text{CH}_3)_3\text{COOH}$ , which has no  $\alpha$ -hydrogen. All results are consistent with the  $\text{E}_{\text{CO}2}$  mechanism, transition state structure, and reaction energy diagrams calculated using the hybrid density functional B3LYP approach. Isotope labeling for  $\text{HO}^- + \text{CH}_3\text{OOH}$  also reveals some interaction between  $\text{H}_2\text{O}$  and  $\text{HO}^-$  within the  $\text{E}_{\text{CO}2}$  product complex  $[\text{H}_2\text{O} \cdots \text{CH}_2=\text{O} \cdots \text{HO}^-]$ . There is little evidence, however, for the formation of the most exothermic products  $\text{H}_2\text{O} + \text{CH}_2(\text{OH})\text{O}^-$ , which would arise from nucleophilic condensation of  $\text{CH}_2=\text{O}$  and  $\text{HO}^-$ . The results suggest that the product dynamics are not totally statistical but are rather direct after the  $\text{E}_{\text{CO}2}$  transition state. The larger  $\text{HO}^- + \text{CH}_3\text{CH}_2\text{OOH}$  system displays more statistical behavior during complex dissociation.

### Introduction

Base-induced  $\text{E}_{\text{CO}2}$  elimination of alkyl peroxides  $\text{X}^- + \text{R}^1\text{R}^2\text{HCOOR}^3 \rightarrow \text{HX} + \text{R}^1\text{R}^2\text{C}=\text{O} + \text{R}^3\text{O}^-$  is a variant of concerted E2 elimination reactions. The mechanism was proposed for solution reactions more than 50 years ago by Kornblum and DeLaMare;<sup>1</sup> the reaction initiates via an attack of a base anion ( $\text{X}^-$ ) on an  $\alpha$ -hydrogen<sup>1,2</sup> similar to the conventional E2 transformation. Unlike E2 reactions forming C=C double bonds, however,  $\text{E}_{\text{CO}2}$  reactions produce stable carbonyl C=O bonds and can be quite exothermic. The  $\text{E}_{\text{CO}2}$  reaction is considerably less explored in part because it is limited to peroxides (and a few other species such as methylnitrite<sup>3</sup> ( $\text{CH}_3\text{ONO}$ ) and dimethyl methylphosphonate<sup>4</sup>  $[(\text{CH}_3\text{O})_2(\text{CH}_3)\text{PO}]$ ), but it could have important implications.<sup>5</sup> For example, polyunsaturated fatty acid residues of phospholipids are extremely sensitive to oxidation during biochemical oxidative stress.<sup>6–8</sup> If lipid peroxides undergo  $\text{E}_{\text{CO}2}$  reactions, they will be converted to highly genotoxic, unsaturated aldehydes and ketones<sup>9,10</sup> that are causative sources for cancer, aging, and pathology.<sup>6,8,11</sup> Despite the potential biochemical interest, the anionic  $\text{E}_{\text{CO}2}$  mechanism of peroxide decomposition has been controversial in solution and in vivo because trace amounts of transition metal ions can afford an analogous product distribution via Fenton chemistry.<sup>2,12</sup>

Recently, a model reaction of  $\text{F}^- + \text{CH}_3\text{OOH} \rightarrow \text{HF} + \text{CH}_2=\text{O} + \text{HO}^-$  has been studied in the gas phase<sup>5</sup> in which interferences due to adventitious metal ions or solvent molecules

have been rigorously eliminated. The gas phase results are totally consistent with the proposed  $\text{E}_{\text{CO}2}$  mechanism, and the following intriguing features are observed for the  $\text{E}_{\text{CO}2}$  reactivity: The measured rate constant is about 50% of the ion-molecule collision rate.<sup>5</sup> The calculated potential energy diagram indicates (i) a transition state significantly below the reactant energy, (ii) an extremely shallow potential well for the pre-reaction complex, and (iii) a large amount of energy release after the  $\text{E}_{\text{CO}2}$  transition state.<sup>5</sup> The rapidity of the reaction may well be rationalized in terms of the transition state energy that supports favorable kinetics. Furthermore, following the  $\text{E}_{\text{CO}2}$  transformation, the hydroxide anion appears to leave the product complex  $[\text{HF} \cdots \text{CH}_2\text{O} \cdots \text{HO}^-]$  without undergoing condensation with formaldehyde to form the most stable product pair  $\text{HF} + \text{CH}_2(\text{OH})\text{O}^-$ .<sup>5</sup> The deep potential well minimum in the product potential energy surface seems to be avoided, in analogy to the  $\text{S}_{\text{N}}2$  reaction of  $\text{HO}^- + \text{CH}_3\text{F}$ .<sup>13</sup> Most recently, Hase and coworkers conducted a direct dynamics trajectory study of this reaction that supported the experimental observations.<sup>14</sup> The post-transition state dynamics do not follow the intrinsic reaction coordinate (IRC) path, which forms the  $[\text{CH}_2(\text{OH})_2 \cdots \text{F}^-]$  potential energy minimum on the IRC, with a 105 kcal mol<sup>-1</sup> reaction exothermicity and, subsequently, the dissociation products  $\text{CH}_2(\text{OH})\text{O}^- + \text{HF}$  with an energy release of 63 kcal mol<sup>-1</sup>. Instead, formation of  $\text{HF} + \text{CH}_2\text{O} + \text{HO}^-$  with an energy release of 27 kcal mol<sup>-1</sup> is the major reaction channel.<sup>14</sup>

Intrinsic efficiencies of base-induced decomposition and the product dynamics, however, are yet to be fully characterized experimentally. For instance, it is unknown why the  $\text{F}^- + \text{CH}_3\text{OOH}$  rate constant is considerably below the collision limit, even though it is fairly rapid;<sup>5</sup> the energetics around the key transition state would suggest a significantly higher reaction

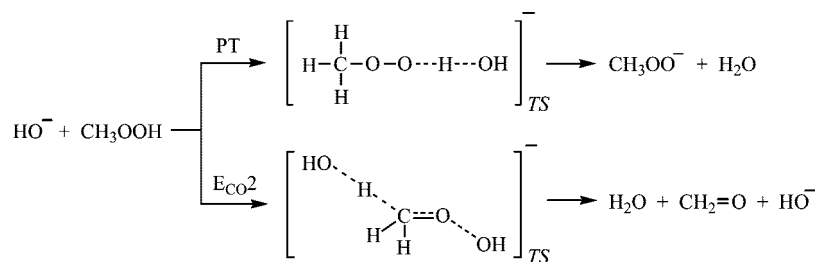
<sup>†</sup> Part of the "Stephen R. Leone Festschrift".

\* Corresponding authors: Shuji.Kato@colorado.edu.; blanksby@uow.edu.au.

<sup>‡</sup> University of Colorado and JILA.

<sup>§</sup> University of Wollongong.

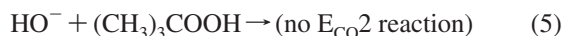
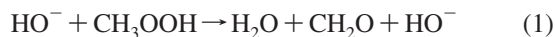
## SCHEME 1



efficiency. It was conjectured that the apparently smaller-than-unity efficiency of the  $\text{F}^- + \text{CH}_3\text{OOH}$  reaction may be due to  $\text{HO}^-$  abstracting a proton from HF within the dissociation complex, thereby regenerating the  $\text{F}^-$  reactant, in effect a novel anion-catalyzed decomposition reaction.<sup>5</sup> It then follows that another type of product dynamics involving an interaction between  $\text{HO}^-$  and HF may need to be considered. We have extended the study of base-induced decomposition of alkyl hydroperoxides to the reactions of superoxide<sup>15</sup> and reported direct observation of the Haber–Weiss reaction in the gas phase; the reaction has been controversial in solution over many decades. The superoxide reactions are also efficient, and produce another major product of ozonide presumably via a mechanism associated with the open-shell character of the reagent base anion.<sup>15</sup>

In the present paper we study the ion–molecule reaction of the hydroxide anion with methyl hydroperoxide to further characterize the base-induced chemical transformation that can now be observed in the isolation of the gas phase. The  $\text{HO}^-$  anion is more basic than  $\text{F}^-$  so that the reaction is expected to involve an exothermic proton transfer (PT) channel as well (Scheme 1). Competition between the PT and  $\text{E}_{\text{CO}2}$  pathways is viewed as an internal prognosticator for the efficiency of the  $\text{E}_{\text{CO}2}$  reaction. Theoretical calculations indicate that the rate-determining energetics, i.e., from the reactants to the pre-reaction complex to the  $\text{E}_{\text{CO}2}$  transition state, are remarkably similar between the  $\text{F}^- + \text{CH}_3\text{OOH}$  and  $\text{HO}^- + \text{CH}_3\text{OOH}$  reactions. Following the  $\text{E}_{\text{CO}2}$  transition state, the  $\text{HO}^- + \text{CH}_3\text{OOH}$  system is significantly more downhill energetically than  $\text{F}^- + \text{CH}_3\text{OOH}$ , and non-statistical behavior may be persistent or even more pronounced.

The  $\text{E}_{\text{CO}2}$  pathway yields the same ionic product as the reactant anion. Isotope analogs are used to differentiate the reaction products and mechanism and to extract the intrinsic efficiency of the  $\text{E}_{\text{CO}2}$  reaction (eqs 1, 2, and 3). The site-specific isotope labeling also allows for quantitative elucidation of dynamical processes occurring within the product complex. The  $\text{E}_{\text{CO}2}$  reaction is studied for a larger system of ethyl hydroperoxide (eq 4), and the effects of size and complexity on the dynamics are examined. The reaction of  $\text{HO}^-$  with *tert*- $\text{C}_4\text{H}_9\text{OOH}$  (eq 5), which bears no  $\alpha$ -hydrogen, is also studied for comparison and completeness.



## Experimental Section

All reactions in the present study used hydroxide anions  $\text{HO}^-$ , not  $\text{DO}^-$ , to elucidate the occurrence of  $\text{E}_{\text{CO}2}$  mechanisms as

well as the product dynamics after the key transition state. Reactions with  $\text{DO}^-$  could produce the same ionic product as is derived from the  $\text{E}_{\text{CO}2}$  scheme, via potential exchange at the peroxy terminus, e.g.,  $\text{DO}^- + \text{CH}_3\text{OOH} \rightarrow [\text{CH}_3\text{OO}^- \cdots \text{HOD}] \rightarrow [\text{CH}_3\text{OOD} \cdots \text{HO}^-] \rightarrow \text{CH}_3\text{OOD} + \text{HO}^-$ . Hydroxide anions were generated in the source section of the selected ion flow tube (SIFT) instrument,<sup>16,17</sup> mass selected, and injected into the reaction flow tube (0.5 Torr He), where the anions are collisionally thermalized to room temperature ( $\approx 300$  K) before ion–molecule reactions initiate. Methyl and ethyl hydroperoxides were synthesized as described previously.<sup>18</sup> *tert*-Butyl hydroperoxide was purchased as a commercial sample (Aldrich) and used without further purification except for drying to remove water. Extreme care was taken in the preparation, handling, and storage of these unstable and potentially explosive compounds. The neutral reagents were introduced into the reaction flow tube to react with  $\text{HO}^-$ , and ionic species were detected with the mass filter located at the downstream end of the flow tube.

Measurements were made after flowing the peroxide reagent for typically 20 minutes or longer in the stream of  $\text{HO}^-$  until the entire inlet system was adequately passivated and conditioned to reach a stationary state as monitored by the mass spectrometer. This was also important to evaporatively remove diethyl ether, a major synthetic impurity in methyl and ethyl hydroperoxides. In a separate experiment, the reaction of diethyl ether with  $\text{HO}^-$  produced comparable amounts of  $\text{C}_2\text{H}_5\text{O}^-$  and  $\text{C}_2\text{H}_5\text{O}^-(\text{H}_2\text{O})$  at  $m/z$  45 and  $m/z$  63, respectively, essentially duplicating previous results.<sup>19–22</sup> A small amount of the signature product  $m/z$  63 was indeed observed in the beginning of passivation with the synthetic alkyl hydroperoxides. The peroxide reagent flows were maintained until the  $m/z$  63 species largely disappeared.

Kinetics measurements with  $\text{HO}^-$  were performed by adding a constant flow of alkyl hydroperoxide via multiple inlets located along the reaction flow tube. Depletion of  $\text{HO}^-$  and formation of ionic products was monitored as a function of the inlet position, which determines the reaction time. Mass discrimination effects were minimized across the mass range for the products, but no further corrections were made. Although the reactions take place in a pseudo-first-order fashion with a large excess of the neutral reagents, complications arise in the kinetics of alkyl hydroperoxides with  $\text{HO}^-$ . For a non-labeled hydroxide reactant, a major and characteristic  $\text{E}_{\text{CO}2}$  product is the same hydroxide anion. Secondary reactions, which are in many cases  $\text{E}_{\text{CO}2}$  reactions, also usually occur extensively for these reactive species. The reaction rate constants and branching ratios for primary products were thus determined from analysis of the kinetics using extrapolation to zero reaction time combined with a full coupled rate equation approach. Product yields (%) are presented as derived from the intrinsic primary branching. Reaction efficiency is defined as the ratio of the measured rate constant to the calculated collision rate constant. For the  $\text{H}^{18}\text{O}^- + \text{CH}_3\text{OOH}$  reaction, the reactant anion  $\text{H}^{18}\text{O}^-$  was mass-selected from  $\text{HO}^-$  at natural abundance in the source flow tube.

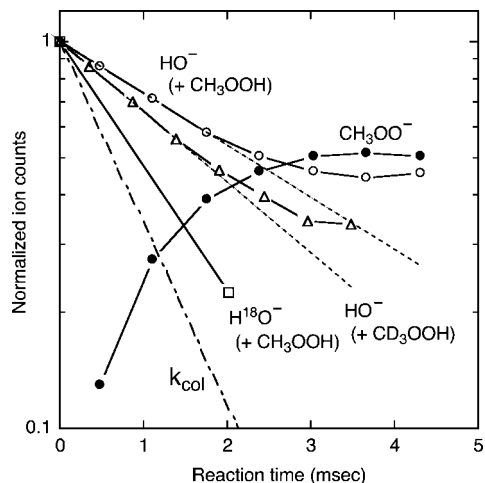


**Figure 1.** Kinetic decays of hydroxide anions in the reactions of  $\text{HO}^- + \text{CH}_3\text{OOH}$  (open circle),  $\text{HO}^- + \text{CD}_3\text{OOH}$  (triangle), and  $\text{H}^{18}\text{O}^- + \text{CH}_3\text{OOH}$  (square). The  $\text{CH}_3\text{OO}^-$  product from the  $\text{HO}^- + \text{CH}_3\text{OOH}$  reaction (closed circle) is also shown. The reaction times have been normalized to account for the different concentrations of methyl hydroperoxide reactants used in these experiments. The dash-dot line indicates the predicted decay of  $\text{HO}^-$  at the collision rate  $k_{\text{col}}$ .

Because of the low ion intensity, regular ion kinetics measurements were not performed. Instead, the reaction was examined back-to-back with the non-labeled  $\text{H}^{16}\text{O}^- + \text{CH}_3\text{OOH}$  reaction. Given the same flow rate of the same neutral reagent, semi-logarithmic depletions of  $\ln[\text{H}^{18}\text{O}^-]/[\text{H}^{18}\text{O}^-]_0$  and  $\ln[\text{H}^{16}\text{O}^-]/[\text{H}^{16}\text{O}^-]_0$  were measured, and the relative rate constant for  $\text{H}^{18}\text{O}^-$  was determined.

Stated error bars in rate constants represent one standard deviation of repeated measurements. The experimental rate constants also usually contain absolute uncertainties of  $\pm 20\%$  due to the overall measurement procedures.<sup>16,17</sup> The systematic errors, however, cancel in comparing the rate constants for different alkyl hydroperoxide reactions. Furthermore, examinations of several simple exothermic reactions in comparison with both literature values and calculated collision rate constants indicate that the absolute error bars are substantially smaller in this study. Systematic uncertainties due to sample purity cannot be entirely eliminated, however. Despite all efforts to minimize impurities and in situ decomposition of the reagents, it is possible that the alkyl hydroperoxides are not 100% pure in the flow tube. Non-reactive impurities will slightly reduce the reaction efficiency. It should thus be noted that experimental reaction efficiencies may still be their lower limits.

Geometry optimizations were carried out with the B3LYP method<sup>23,24</sup> using the modest 6-31+G(d) basis set within the GAUSSIAN03 suite of programs.<sup>25</sup> All stationary points of the potential energy surfaces were characterized as either minima (no imaginary frequencies) or transition states (one imaginary frequency) by calculation of the frequencies using analytical gradient procedures. Frequency calculations provided zero-point energies, which were corrected by the empirical scaling factor of 0.9804 and added to the calculated electronic energy.<sup>26</sup> For the  $\text{HO}^- + \text{CH}_3\text{OOH}$  potential (Figure 2) the minima connected by a given transition state were confirmed by IRC calculations<sup>27,28</sup> while for the  $\text{HO}^- + \text{CH}_3\text{CH}_2\text{OOH}$  potential (Figure 4) the connectivity was assigned by comparison of transition states with their methyl analogues and by inspection of the animated imaginary frequencies using the Gaussview or MOLDEN<sup>29</sup> packages. In some instances, single point energy calculations were conducted on each of the stationary point geometries using

the CCSD(T) method<sup>30</sup> and the correlation consistent basis set aug-cc-pVDZ.<sup>31</sup> The electronic energies, zero-point energies, and geometries of important stationary points are provided as Supporting Information.

Collision rate constants were evaluated via the parametrized trajectory collision rate theory<sup>32</sup> using the polarizabilities<sup>33</sup> of  $4.05$ ,  $5.85$ , and  $9.50 \times 10^{-24} \text{ cm}^3$  and electric dipole moments of  $1.66$ ,  $1.77$ , and  $1.84 \text{ D}$  calculated at B3LYP/6-31+G(d)<sup>25</sup> for  $\text{CH}_3\text{OOH}$ ,  $\text{C}_2\text{H}_5\text{OOH}$ , and *tert*- $\text{C}_4\text{H}_9\text{OOH}$ , respectively.

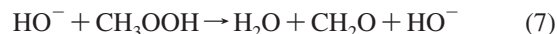
## Results

**$\text{HO}^- + \text{CH}_3\text{OOH}$  Reaction.** Figure 1 shows the kinetics decay of the hydroxide anion in the reaction of  $\text{HO}^- + \text{CH}_3\text{OOH}$  (eqs 6 and 7).  $\text{CH}_3\text{OO}^-$  is the major product ( $\approx 92\%$ ) formed from exothermic proton transfer ( $\Delta_{\text{rxn}}H_{298} = -15.7 \text{ kcal mol}^{-1}$ ).<sup>18,34</sup>

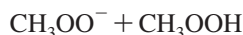


A small amount of methoxide anion ( $\approx 8\%$ ) is the other observed product. It was seen that all alkyl hydroperoxides in the present study formed minor amounts of corresponding alkoxide anions (6–8%). The formation mechanism is unknown (see below), and the alkoxide channels will not be explicitly shown in the equations and schemes.

A strong deviation from linearity is observed in the later stage of the semi-logarithmic kinetics plot (Figure 1). Two features are clearly seen. First, the initial decay of  $\text{HO}^-$  is unusually slow for this highly exothermic proton transfer system. The rate constant is determined from the initial slope to be  $k = 7.6 \pm 0.2 \times 10^{-10} \text{ cm}^3 \text{ s}^{-1}$ , accounting for only 29% of the calculated collision rate ( $2.64 \times 10^{-9} \text{ cm}^3 \text{ s}^{-1}$ ). This strongly suggests the occurrence of a competing  $\text{E}_{\text{CO}2}$  pathway (eq 7), which invisibly reproduces  $\text{HO}^-$ .



Secondly, the decay of  $\text{HO}^-$  eventually stops as the  $\text{CH}_3\text{OO}^-$  signal reaches a plateau at about a 50% height (Figure 1), establishing a constant ratio between the two anions. This is caused by the facile secondary reaction of  $\text{CH}_3\text{OO}^-$  that regenerates the  $\text{HO}^-$  reactant via an  $\text{E}_{\text{CO}2}$  mechanism (eqs 8 and 9).



Methyl peroxide anion ( $\Delta_{\text{acid}}H_{298}(\text{CH}_3\text{OOH}) = 374.6 \text{ kcal mol}^{-1}$ ) is even more basic than  $\text{F}^-$  ( $\Delta_{\text{acid}}H_{298}(\text{HF}) = 371.3 \text{ kcal mol}^{-1}$ ) and is expected to be  $\text{E}_{\text{CO}2}$  active. Because of the chemical reactivity, the formation of a simple adduct  $\text{CH}_3\text{OO}^-(\text{CH}_3\text{OOH})$  is very minor, as observed experimentally.

**$\text{HO}^- + \text{CD}_3\text{OOH}$  Reaction.** The kinetics plot for the decay of  $\text{HO}^-$  with  $\text{CD}_3\text{OOH}$  is also displayed in Figure 1. While similar deviation from linearity is observed, the decay of  $\text{HO}^-$  is faster with  $\text{CD}_3\text{OOH}$  than with  $\text{CH}_3\text{OOH}$ . The rate constant is determined from the initial slope to be  $k = 10.2 \pm 0.2 \times 10^{-10} \text{ cm}^3 \text{ s}^{-1}$  (efficiency of 39% with respect to the collision rate). In addition to the proton-transfer product  $\text{CD}_3\text{OO}^-$  ( $\approx 80\%$ ),  $\text{DO}^-$  is observed among the products.  $\text{DO}^-$  is formed presumably via intracomplex H/D exchange following the initial  $\text{E}_{\text{CO}2}$  transformation (eqs 11 and 12).<sup>5</sup>

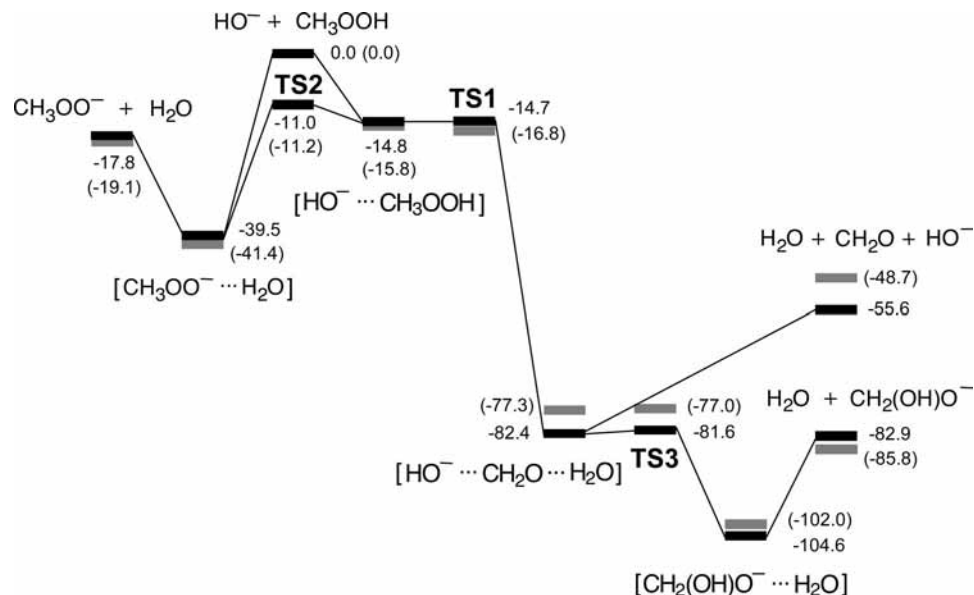


**Figure 2.** Relative energies (kcal mol<sup>-1</sup>) on the [HO<sup>-</sup>, CH<sub>3</sub>OOH] potential energy surface (electronic energy + zero-point energy) calculated at CCSD(T)/aug-cc-pVDZ//B3LYP/6-31+G(d). B3LYP/6-31+G(d) energies are also indicated in parentheses. All energies include a scaled (0.9804) zero-point energy correction.

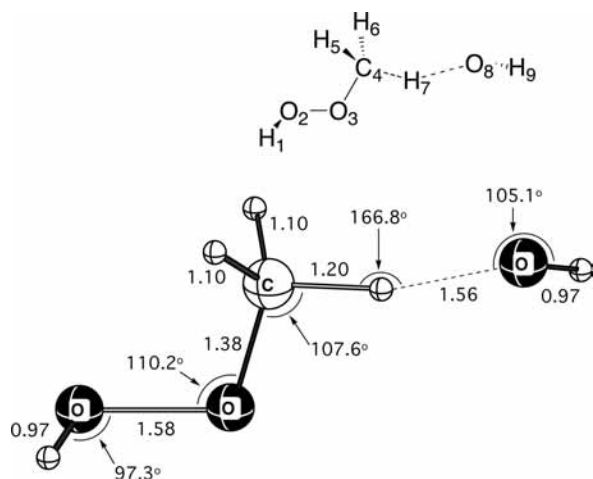
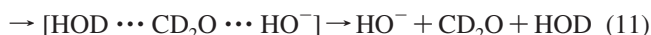
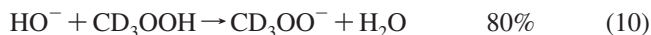


**Figure 3.** Structure of the ECo2 transition state (TS1) for the HO<sup>-</sup> + CH<sub>3</sub>OOH reaction calculated at the B3LYP/6-31+G(d) level of theory.



13% (12)

In the later stage of the kinetics, the HO<sup>-</sup> signal reaches a lower plateau than that observed in the HO<sup>-</sup> + CH<sub>3</sub>OOH reaction (Figure 1), while the proton-transfer product CD<sub>3</sub>OO<sup>-</sup> has a plateau at about the same height of 50%. Formation of the additional DO<sup>-</sup> product mostly accounts for the faster decay of the parent ion. The results suggest that the faster reaction of HO<sup>-</sup> + CD<sub>3</sub>OOH is facilitated primarily by the formation of the additional visible product through post-transition state H/D exchange, and not by a difference in the rate kinetics at the

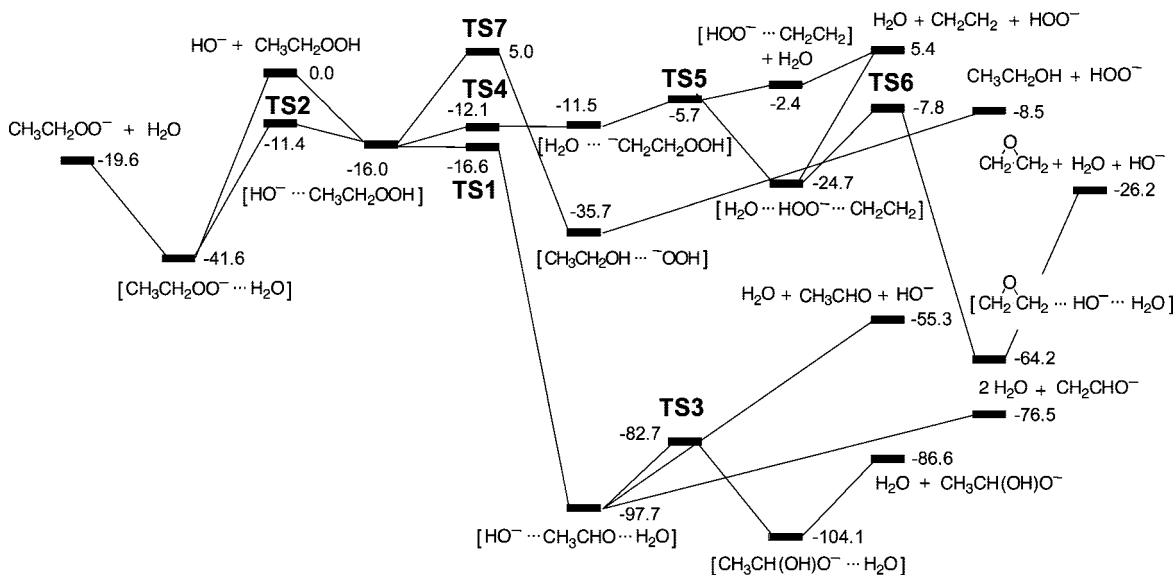
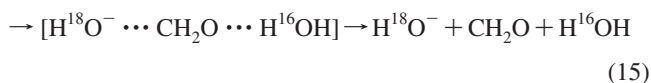
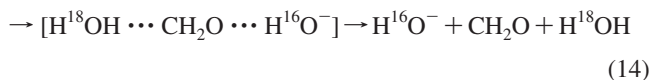


**Figure 4.** Relative energies (kcal mol<sup>-1</sup>) on the [HO<sup>-</sup>, CH<sub>3</sub>CH<sub>2</sub>OOH] potential energy surface (electronic energy + zero-point energy) calculated at B3LYP/6-31+G(d). All energies include a scaled (0.9804) zero-point energy correction.

$E_{CO2}$  barrier (or by a possible difference in the reagent purities between  $CH_3OOH$  and  $CD_3OOH$ ). Primary deuterium kinetic isotope effects (KIEs) would instead favor  $E_{CO2}$  elimination of  $CH_3OOH$  over that of  $CD_3OOH$ . As will be discussed later, the intrinsic KIEs are likely very small for these systems.

The  $HO^- + CD_3OOH$  reaction also produced a trace amount ( $< 1\%$ ) of species at  $m/z$  46, which is assigned to deuterated formate  $DCO_2^-$ .<sup>35</sup> The formate anion is an intrinsic product from the reaction and not due to deprotonation of formic acid  $DCOOH$ , a possible contaminant. Our experiment on the  $HO^- + HCOOH$  reaction yielded two anionic products,  $HCO_2^-$  and  $HO^-(H_2O)$ , with the ratio of  $\sim 3:1$ , as similarly reported by Tanner et al.<sup>36</sup> The  $DCO_2^-$  anion was observed from the  $HO^- + CD_3OOH$  reaction, whereas  $HO^-(HDO)$ , the signature species for  $DCOOH$ , was missing.

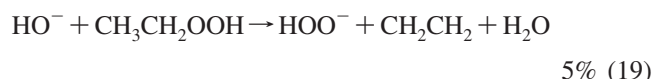
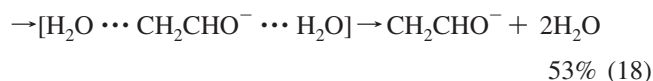
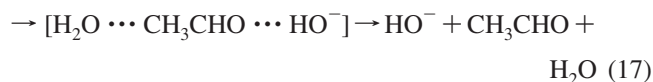
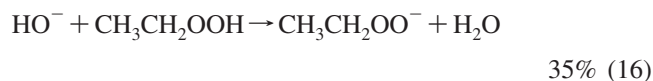
**$H^{18}O^- + CH_3OOH$  Reaction.** The rate of loss for  $H^{18}O^-$  is  $2.4 \pm 0.1$  times faster than the rate of loss for  $HO^-$  in the reaction with  $CH_3OOH$ , as measured in the linear regime of the kinetics (Figure 1). This result gives the rate constant of  $k = 18.0 \pm 0.9 \times 10^{-10} \text{ cm}^3 \text{ s}^{-1}$ , considerably closer to the collision rate (efficiency 71%). Approximately 40% of  $H^{16}O^-$  is formed with respect to the parent ion loss (eq 14), consistent with the  $E_{CO2}$  reaction scheme in which the anion abstracts an  $\alpha$ -hydrogen on the methyl group with concerted elimination of the terminal hydroxide anion as the product.



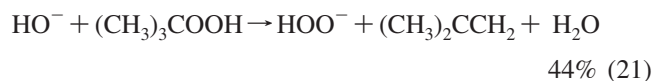
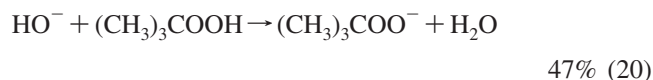
In analogy to the  $HO^- + CD_3OOH$  reaction, intracomplex proton exchange must be occurring to regenerate the  $H^{18}O^-$  reactant (eq 15).

**$HO^- + CH_3CH_2OOH$  Reaction.** The measured rate constant is  $k = 12.9 \pm 0.2 \times 10^{-10} \text{ cm}^3 \text{ s}^{-1}$  with an efficiency of 45%. Proton transfer (eq 16) is a major reaction observed. The  $E_{CO2}$  reaction (eq 17) is invisible, but intracomplex rearrangement can yield deprotonated acetaldehyde (eq 18), the other major product observed. A minor amount of  $HOO^-$  is attributed to a competing elimination reaction with abstraction of a  $\beta$ -hydrogen

from  $C_2H_5OOH$  (eq 19). Nucleophilic substitution at the  $\alpha$ -carbon could also conceivably produce  $HOO^-$  (see Table 1) but is excluded based on the absence of this product channel in the  $HO^- + CH_3OOH$  system. The overall reaction is relatively slow despite the exothermic proton transfer ( $\Delta_{rxn}H_{298} = -19.3 \text{ kcal mol}^{-1}$ ). This result is explained by the invisible  $E_{CO2}$  channel to regenerate  $HO^-$ , thereby apparently slowing down the overall kinetic decay of  $HO^-$ .



**$HO^- + (CH_3)_3COOH$  Reaction.** The measured rate constant is  $k = 21.0 \pm 1.0 \times 10^{-10} \text{ cm}^3 \text{ s}^{-1}$  (efficiency 69%). Proton transfer (eq 20) is a major reaction observed. The other major product  $HOO^-$  is assigned to a competing elimination reaction (eq 21).<sup>37</sup> The overall reaction still appears to be slow considering the large exothermicity for proton transfer ( $\Delta_{rxn}H_{298} = -20.1 \text{ kcal mol}^{-1}$ ).



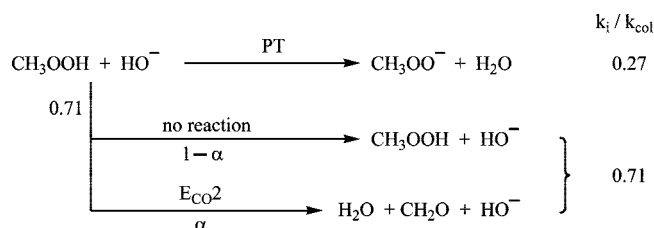
**Kinetic Analysis for Methyl Hydroperoxides.** Reaction schemes for the hydroxide anions can be constructed from the measured rate constants and product distributions (Schemes 2–4). In these schemes, the branching fractions are displayed as the reaction rate for channel  $i$  normalized to the collision rate ( $k_i/k_{col}$ ). In the  $HO^- + CH_3OOH$  reaction, direct proton transfer accounts for 27% of collisions (Scheme 2), while an additional 2% is for methoxide formation (not shown). Seventy-one percent of collisions result in no apparent loss of  $HO^-$ ;

**TABLE 1: Reaction Products and Enthalpies for  $CH_3OOH$ ,  $C_2H_5OOH$ , and *tert*- $C_4H_9OOH$**

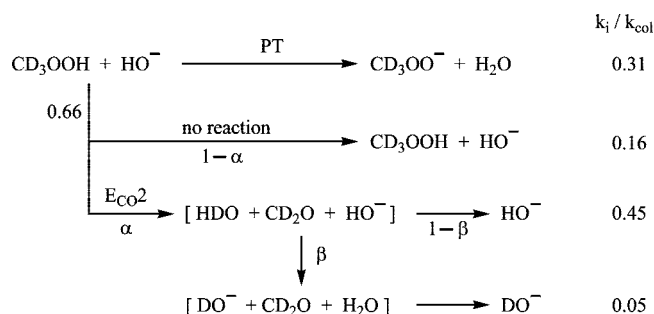
reactants	reaction	products	reaction enthalpy <sup>a</sup>
$CH_3OOH + HO^-$	PT	$CH_3OO^- + H_2O$	$-15.7 (-17.8)^b$
	$E_{CO2}$	$HO^- + CH_2O + H_2O$	$-54.6 (-55.6)^b$
	$S_{N2}(\alpha)$	$HOO^- + CH_3OH$	$-5.6$
$CH_3CH_2OOH + HO^-$	PT	$CH_3CH_2OO^- + H_2O$	$-19.3 (-19.6)^c$
	$E_{CO2}$	$HO^- + CH_3CHO + H_2O$	$-59.1 (-55.3)^c$
	$S_{N2}(\alpha)$	$HOO^- + CH_3CH_2OH$	$-5.2 (-8.5)^c$
	$S_{N2}(\beta)$	$HO^- + CH_2O + CH_3OH$	$-36.2 (-36.8)^c$
	E1cb	$HOO^- + C_2H_4 + H_2O$	$5.7 (5.4)^c$
	epoxidation	$HO^- + \text{cyc-}CH_2CH_2O + H_2O$	$-30.9 (-26.2)^c$
$(CH_3)_3COOH + HO^-$	PT	$(CH_3)_3COO^- + H_2O$	$-20.1$
	$S_{N2}(\alpha)$	$HOO^- + (CH_3)_3COH$	$-5.9$
	$S_{N2}(\beta)$	$HO^- + (CH_3)_2CO + CH_3OH$	$-42.9$
	E2/E1cb	$HOO^- + (CH_3)_2C=CH_2 + H_2O$	$6.7$
	epoxidation	$HO^- + \text{cyc-}CH_2C(CH_3)_2O + H_2O$	not available

<sup>a</sup> All experimental energies in  $\text{kcal mol}^{-1}$  at 298 K.<sup>34</sup> <sup>b</sup> Calculated at CCSD(T)/aug-cc-pVDZ//B3LYP/6-31+G(d) with zero-point energy corrections (scaling factor 0.9804). <sup>c</sup> Calculated at B3LYP/6-31+G(d) with zero-point energy corrections (scaling factor 0.9804).

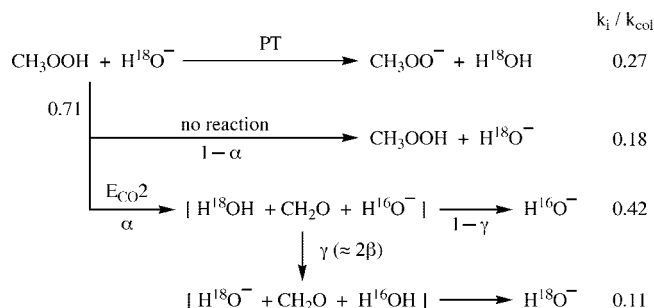
## SCHEME 2



## SCHEME 3



## SCHEME 4



this result is the sum of the invisible E<sub>CO2</sub> pathway ( $\alpha$ ) and non-reactive collisions ( $1 - \alpha$ ).

In the HO<sup>-</sup> + CD<sub>3</sub>OOH reaction (Scheme 3), invisible pathways to give HO<sup>-</sup> must account for 61% of total collisions based on the measured reaction efficiency. With the H/D scrambling scheme, a fraction ( $\beta$ ) of HO<sup>-</sup> converts to DO<sup>-</sup> within the E<sub>CO2</sub> product complex (observed DO<sup>-</sup> branching fraction  $\cong$  5% of collisions). The [DO<sup>-</sup>]/[HO<sup>-</sup>] ratio thus must be  $\alpha\beta/(1 - \alpha\beta) = 0.05/0.61 \cong 0.08$ . Since  $\alpha$  is separately determined to be 0.75 from the H<sup>18</sup>O<sup>-</sup> reaction (see below), the isotope-scrambling probability  $\beta$  is obtained as 0.10. Regeneration of HO<sup>-</sup> via the E<sub>CO2</sub> channel then accounts for  $0.66 \times \alpha(1 - \beta) = 0.45$ , thus giving the probability for non-reactive collision as 16%. Intrinsic reaction efficiencies (including E<sub>CO2</sub> regeneration of HO<sup>-</sup>) are determined to be 84% and 50% for the overall reaction and E<sub>CO2</sub> channel, respectively.

It is reasonable to assume that the H<sup>18</sup>O<sup>-</sup> + CH<sub>3</sub>OOH reaction (Scheme 4) produces the same amount of proton-transfer product CH<sub>3</sub>OO<sup>-</sup> (27%) as the non-labeled HO<sup>-</sup> + CH<sub>3</sub>OOH reaction. It is also a good approximation from the reaction degeneracy that the isotope-scrambling probability to form H<sup>18</sup>O<sup>-</sup> ( $\gamma$ ) is 2 times greater than that forming DO<sup>-</sup>; the very large exothermicity for the E<sub>CO2</sub> pathway ( $\Delta_{\text{rxn}}H_{298} = -54.6 \text{ kcal mol}^{-1}$ ) would diminish isotope effects (kinetic/equilibrium) in the hydroxide-water exchange. From the experimental DO<sup>-</sup> branching fraction of about 5% (Scheme 3), the branching fraction for E<sub>CO2</sub> regeneration of H<sup>18</sup>O<sup>-</sup> must thus be 11%. This requires that  $\alpha\gamma = 0.15$  (Scheme 4). Production of H<sup>16</sup>O<sup>-</sup> from the H<sup>18</sup>O<sup>-</sup> reactant is the origin of the faster reaction of H<sup>18</sup>O<sup>-</sup> + CH<sub>3</sub>OOH as compared to H<sup>16</sup>O<sup>-</sup> + CH<sub>3</sub>OOH, which regenerates

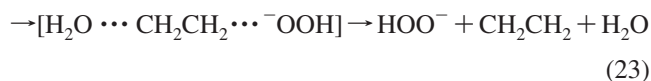
H<sup>16</sup>O<sup>-</sup>. The observed efficiency ratio is 2.5 between these reactions. This places an additional requirement that  $\alpha(1 - \gamma) = 0.60$ .  $\alpha = 0.75$  and  $\gamma = 0.20$  are finally obtained. The branching fractions for H<sup>16</sup>O<sup>-</sup> formation and non-reactive collision are then calculated to be 42% and 18%, respectively (Scheme 4).<sup>38</sup> Intrinsic efficiencies (including E<sub>CO2</sub> regeneration of H<sup>18</sup>O<sup>-</sup>) are determined to be 82% and 53% for the overall reaction and E<sub>CO2</sub> channel, respectively.

## Discussion

**Reaction mechanisms.** Table 1 lists reaction enthalpies for HO<sup>-</sup> reacting with CH<sub>3</sub>OOH, C<sub>2</sub>H<sub>5</sub>OOH, and *tert*-C<sub>4</sub>H<sub>9</sub>OOH. Relative energies on the [HO<sup>-</sup>, CH<sub>3</sub>OOH] potential energy surface are shown in Figure 2 at the B3LYP/6-31+G(d) and CCSD(T)/aug-cc-pVDZ//B3LYP/6-31+G(d) levels of theory. The CCSD(T) computations reproduce experimental heats of reaction particularly well (Table 1), and the computationally cheaper B3LYP calculations agree well with the CCSD(T) results with the exception of product energies involving formaldehyde, suggesting that the hybrid density functional approach should be suitable for larger systems. The computations account for the overall features of the observed reactions. The E<sub>CO2</sub> reaction proceeds via the characteristic transition state (TS1), an anti-periplanar structure that is consistent with the synchronous E2 reaction mechanism (Figure 3). The proton transfer reaction is energetically allowed and highly exothermic. No reaction was observed from CH<sub>3</sub>OO<sup>-</sup> + H<sub>2</sub>O, also consistent with the computations that the reactant energy is lower than both TS1 and the preceding transition state TS2 for rearrangement of the HO<sup>-</sup> species.

At the B3LYP level of theory, the HO<sup>-</sup> + C<sub>2</sub>H<sub>5</sub>OOH reaction (Figure 4) has proton transfer and E<sub>CO2</sub> energetics that are very similar to HO<sup>-</sup> + CH<sub>3</sub>OOH. Proton transfer and E<sub>CO2</sub> reaction enthalpies agree fairly well with experimental values (Table 1). Formation of the <sup>-</sup>CH<sub>2</sub>CHO anion via intracomplex proton transfer (eq 18) is a highly exothermic process ( $\Delta_{\text{rxn}}H_{298}(\text{experimental}) = -83.6 \text{ kcal mol}^{-1}$ ) and is a major product channel observed experimentally. The E<sub>CO2</sub> channel is not available for (CH<sub>3</sub>)<sub>3</sub>COOH because it has no  $\alpha$ -hydrogen; the absence of E<sub>CO2</sub> reactivity has been demonstrated in the similar reaction of F<sup>-</sup> + (CH<sub>3</sub>)<sub>3</sub>COOH.<sup>5</sup>

Both the C<sub>2</sub>H<sub>5</sub>OOH and *tert*-C<sub>4</sub>H<sub>9</sub>OOH reactions show the additional product HOO<sup>-</sup> that is absent from the CH<sub>3</sub>OOH system. This strongly suggests the involvement of  $\beta$ -hydrogens in the reaction. Instead of concerted E2 elimination, a slightly different E1cb mechanism has been identified computationally for HO<sup>-</sup> + C<sub>2</sub>H<sub>5</sub>OOH (eqs 22 and 23).



Here, deprotonated <sup>-</sup>CH<sub>2</sub>CH<sub>2</sub>OOH is a stable structure within the ion-molecule complex as the carbanion is stabilized by the water molecule and intramolecular interaction with the -OOH moiety (Figure 5). Following further rearrangement via TS5 (Figure 4) the E1cb reaction yields the same products as the conventional E2 mechanism. It is interesting to note that in the HO<sup>-</sup> + CH<sub>3</sub>OOH reaction an analogous <sup>-</sup>CH<sub>2</sub>OOH structure is not stable but connects directly to the TS1 transition state. Formation of HOO<sup>-</sup> from HO<sup>-</sup> + *tert*-C<sub>4</sub>H<sub>9</sub>OOH may be via either E2 or E1cb, subtly dependent on the stability of the

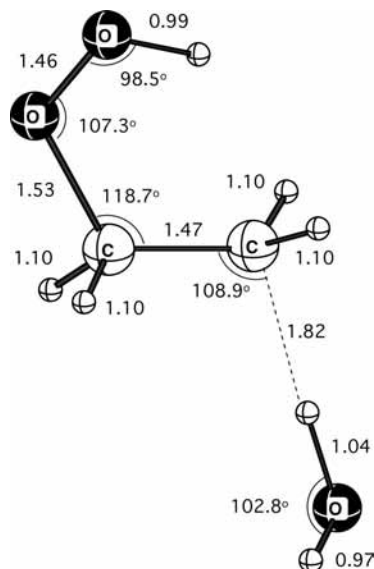


**Figure 5.** Structure of the  $E_{1cb}$  stationary state for the  $\text{HO}^- + \text{CH}_3\text{CH}_2\text{OH}$  reaction calculated at the B3LYP/6-31+G(d) level of theory.

$-\text{CH}_2(\text{CH}_3)_2\text{COOH}$  structure. Notably, overall, the elimination pathways are somewhat endothermic both experimentally and computationally for the  $\text{C}_2\text{H}_5\text{OOH}$  and *tert*- $\text{C}_4\text{H}_9\text{OOH}$  reactions (Table 1). Formation of  $\text{HOO}^-$  can be explained as follows: In the TS5 transition state,  $\text{H}_2\text{O}$  and  $\text{HOO}^-$  are sterically separated by the intervening ethylene species. TS5 could thus dissociate to a product pair of  $[\text{HOO}^- \cdots \text{CH}_2\text{CH}_2]$  and  $\text{H}_2\text{O}$ , with the calculated exothermicity of 2.4 kcal mol $^{-1}$  (Figure 4). The  $[\text{HOO}^- \cdots \text{CH}_2\text{CH}_2]$  product is only weakly bound by 7.8 kcal mol $^{-1}$  so that it will subsequently dissociate to  $\text{HOO}^-$  and  $\text{CH}_2\text{CH}_2$ ; we have observed that ion clusters with binding energies of 15 kcal mol $^{-1}$  or smaller generally do not survive the high-pressure flow tube at room temperature. Alternatively, the B3LYP calculations predict that the reaction is exoergic ( $\Delta_{\text{rxn}}G_{298} = -5.7$  kcal mol $^{-1}$ ) although it is endothermic ( $\Delta_{\text{rxn}}H_{298} = +6.4$  kcal mol $^{-1}$ ) so that the entropy may play a role in promoting these irreversible transformations.

Nucleophilic substitution ( $\text{S}_{\text{N}}2$ ) reactions are energetically accessible for all the alkyl hydroperoxides (Table 1).  $\text{S}_{\text{N}}2$  reactions at  $\alpha$ -carbons are similarly and moderately exothermic ( $\Delta_{\text{rxn}}H_{298} \approx -5$  kcal mol $^{-1}$ ) eliminating  $\text{HOO}^-$ . The  $\text{S}_{\text{N}}2(\alpha)$  reaction, however, does not seem to be competitive with other facile reaction channels;  $\text{HOO}^-$  was not observed from  $\text{CH}_3\text{OOH} + \text{HO}^-$ , which has the least steric hindrance and lowest kinetic barrier<sup>39</sup> towards the  $\text{S}_{\text{N}}2$  transformation  $\text{HO}^- + \text{CH}_3\text{OOH} \rightarrow [\text{HOCH}_3 \cdots \text{OOH}]$ . Sequential intracomplex proton transfer to yield  $\text{CH}_3\text{O}^- + \text{HOOH}$  is even less exothermic ( $-0.1$  kcal mol $^{-1}$ ) and improbable. Given the fact that  $\text{S}_{\text{N}}2(\alpha)$  transformation is even less likely to occur for ethyl and *tert*-butyl hydroperoxides, production of  $\text{C}_2\text{H}_5\text{O}^- + \text{HOOH}$  and *tert*- $\text{C}_4\text{H}_9\text{O}^- + \text{HOOH}$  cannot take place even though they are slightly more exothermic ( $\Delta_{\text{rxn}}H_{298} = -3.4$  and  $-7.7$  kcal mol $^{-1}$ , respectively). The  $\text{S}_{\text{N}}2(\alpha)$  mechanism was investigated computationally for the  $\text{HO}^- + \text{CH}_3\text{CH}_2\text{OOH}$  potential, and the barrier to the reaction (via TS7 in Figure 4) was found to be 5.0 kcal mol $^{-1}$  above the entrance channel. Thus on the basis of experimental and computational observations, the  $\text{S}_{\text{N}}2(\alpha)$  mechanism is unlikely and does not account for the observed formation of  $\text{HOO}^-$  or alkoxide anions.<sup>40,41</sup>  $\text{S}_{\text{N}}2$  reactions at  $\beta$ -carbons (e.g.,  $\text{HO}^- + \text{CH}_3\text{CH}_2\text{OOH} \rightarrow [\text{HOCH}_3 \cdots \text{CH}_2\text{OOH}] \rightarrow \text{CH}_3\text{OH} + \text{CH}_2\text{O} + \text{HO}^-$ ) are highly exothermic in

ethyl and *tert*-butyl reactions (Table 1). The barrier to this process, however, is very high, and the  $\text{S}_{\text{N}}2(\beta)$  mechanism should be excluded; the associated transition state for the ethyl reaction (TS8, Supporting Information) is 74.3 kcal mol $^{-1}$  higher in energy relative to the reactants.

We computationally identify yet another pathway for  $\text{HO}^- + \text{C}_2\text{H}_5\text{OOH}$  that yields ethylene oxide and regenerates hydroxide via TS6 (Figure 4). Along the reaction energy diagram, all intermediates and transition states are below the reactants. IRC analysis indicates that TS6 does connect the  $[\text{H}_2\text{O} \cdots \text{HOO}^- \cdots \text{CH}_2\text{CH}_2]$  complex with the epoxide complex. A similar mechanism with *tert*- $\text{C}_4\text{H}_9\text{OOH}$  would form 2,2-dimethyl oxirane *cyc*- $\text{CH}_2\text{C}(\text{CH}_3)_2\text{O}$ . In collision-induced dissociation of  $\text{C}_2\text{H}_5\text{OO}^-$  and *tert*- $\text{C}_4\text{H}_9\text{OO}^-$  anions, analogous formation of epoxides is a plausible and significant mechanism for the observed production of  $\text{HO}^-$  at relatively high collision energies.<sup>42</sup> If the epoxide pathway is occurring substantially in the  $\text{HO}^- + \text{C}_2\text{H}_5\text{OOH}$  and *tert*- $\text{C}_4\text{H}_9\text{OOH}$  reactions, it provides an additional mechanism to account for the apparent slowness of the overall reactions below the collision rates.

**Intrinsic  $\text{E}_{\text{CO}2}$  Efficiencies.** The isotope labeling revealed the overall efficiency for the  $\text{HO}^- + \text{CH}_3\text{OOH}$  reaction to be 80% or greater (recall that the efficiency is the lower limit if non-reactive impurities are present in the neutral reagent; see Experimental Section) The  $\text{E}_{\text{CO}2}$  decomposition is the major process (efficiency  $\approx 50\%$  of collision), whereas proton transfer is less effective ( $\approx 30\%$  of collision). For comparison, in the  $\text{F}^- + \text{CH}_3\text{OOH}$  reaction,<sup>5</sup> the  $\text{E}_{\text{CO}2}$  reactivity represents most of the overall efficiency (49%), while proton transfer is slightly endothermic and only an upper bound is given for the efficiency ( $<5\%$ ). The  $\text{HO}^- + \text{CH}_3\text{OOH}$  reaction is a rare example in which a competing chemical pathway predominates over an exothermic, barrierless proton transfer that would otherwise proceed at unit efficiency.<sup>43</sup> Associative detachment may similarly compete with proton transfer in the reaction of *o*-benzynes with  $\text{HO}^-$ .<sup>44,45</sup> From the other perspective, the  $\text{E}_{\text{CO}2}$  reactivity could even approach unit efficiency if proton transfer were not competing. The high efficiency may be understood in terms of the energetics around the TS1 transition state, which is 14.7 kcal mol $^{-1}$  lower in energy than the reactants at the CCSD(T) level of theory and follows an extremely shallow pre-reaction complex well ( $-14.8$  kcal mol $^{-1}$ ). The energetics compare well with those for  $\text{F}^- + \text{CH}_3\text{OOH}$ ; the pre-reactive complex and the transition state are 15.9 and 14.6 kcal mol $^{-1}$  lower in energy than the reactants, respectively, at the same level of theory.<sup>5</sup> Once the pre-reaction complex is formed from  $\text{CH}_3\text{OOH}$  and  $\text{HO}^-$  (or  $\text{F}^-$ ), access to the TS1 transition state should be facile. Such unusually shallow wells for the pre-reaction complexes (0.1 and 1.3 kcal mol $^{-1}$  relative to the transition states for  $\text{HO}^-$  and  $\text{F}^-$ , respectively) suggest that their lifetimes may be sufficiently short so that intramolecular vibrational energy redistribution is incomplete and, thus, their unimolecular kinetics are non-RRKM.<sup>46,47</sup> Addressing this intriguing question is beyond the scope of the experimental and computational approach in this study.

The calculated bond lengths indicate subtle but important differences between the  $\text{HO}^- + \text{CH}_3\text{OOH}$  and  $\text{F}^- + \text{CH}_3\text{OOH}$  reactions. The TS1 for  $\text{HO}^- + \text{CH}_3\text{OOH}$  is even closer to the reactants (free  $\text{CH}_3\text{OOH}$ ) than is the TS1 for  $\text{F}^- + \text{CH}_3\text{OOH}$  (Table 2).<sup>48,49</sup> At the transition state, the C–H and O–O bonds are elongated by only about 0.1 Å (as compared to  $\approx 0.2$  Å for  $\text{F}^-$ ), while the C–O bond is shortened by only about 0.04 Å ( $\approx 0.08$  Å for  $\text{F}^-$ ). The TS1 for  $\text{HO}^- + \text{CH}_3\text{OOH}$  is thus characterized by a very early transition state, qualitatively

**TABLE 2: Bond Lengths (Å) for E<sub>CO2</sub> Transformations of CH<sub>3</sub>OOH and CH<sub>3</sub>CH<sub>2</sub>OOH<sup>a</sup>**

structure	O8–H7 <sup>b</sup>	H7–C4	C4–O3	O3–O2
<b>CH<sub>3</sub>OOH + HO<sup>-</sup> reaction</b>				
CH <sub>3</sub> OOH		1.095	1.419	1.461
			1.437 <sup>c</sup>	1.443 <sup>c</sup>
[HO <sup>-</sup> ···CH <sub>3</sub> OOH]	1.689	1.159	1.407	1.476
TS1 (HO <sup>-</sup> + CH <sub>3</sub> OOH)	1.561	1.200	1.384	1.577
<b>CH<sub>3</sub>OOH + F<sup>-</sup> reaction</b>				
[F <sup>-</sup> ···CH <sub>3</sub> OOH]	1.647 <sup>b</sup>	1.142	1.417	1.495
TS1 (F <sup>-</sup> + CH <sub>3</sub> OOH)	1.272 <sup>b</sup>	1.303	1.341	1.686
<b>CH<sub>3</sub>CH<sub>2</sub>OOH + HO<sup>-</sup> reaction</b>				
CH <sub>3</sub> CH <sub>2</sub> OOH		1.097	1.429	1.460
[HO <sup>-</sup> ···CH <sub>3</sub> CH <sub>2</sub> OOH]	1.696	1.157	1.408	1.533
TS1 (HO <sup>-</sup> + CH <sub>3</sub> CH <sub>2</sub> OOH)	1.623	1.179	1.393	1.568

<sup>a</sup> Calculated at B3LYP/6-31+G(d). The numbering of the nuclei is shown in Figure 3. In all structures, the attacking anion is attached to an α-hydrogen (H7). <sup>b</sup> F8–H7 lengths for CH<sub>3</sub>OOH + F<sup>-</sup>. <sup>c</sup> Experimental.<sup>48,49</sup>

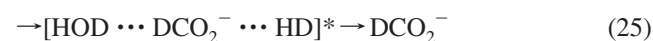
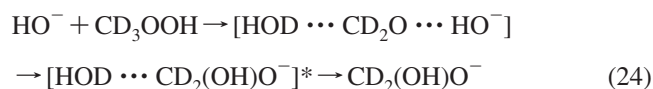
consistent with the significantly larger reaction exothermicity (54.6 kcal mol<sup>-1</sup>, in comparison to 35.6 kcal mol<sup>-1</sup> for F<sup>-</sup> + CH<sub>3</sub>OOH). A similar conclusion can be drawn for HO<sup>-</sup> + CH<sub>3</sub>CH<sub>2</sub>OOH (Table 2). The *intrinsic* primary deuterium KIE for E<sub>CO2</sub> transformations of HO<sup>-</sup> + CH<sub>3</sub>OOH versus HO<sup>-</sup> + CD<sub>3</sub>OOH is thus expected to be very small, while it can still be normal ( $k_H/k_D > 1$ ), typical of concerted E2 reactions. In addition, the overall reaction efficiencies including proton transfer are sufficiently large that they approach saturation. These factors should combine to make the overall KIE very close to unity for ensembles immediately after the TS1 transition states. While moderately rapid E2 reactions of diethyl ether display KIE values of 2–7 in the gas phase at ambient temperature,<sup>20,22,50</sup> the KIE values are essentially unity for rapid E2 reactions of *tert*-butyl halides.<sup>51</sup> This argument justifies the assignment that the observed faster reaction of HO<sup>-</sup> + CD<sub>3</sub>OOH (and hence the apparently inverse KIE) reflects, in reality, the post-transition state H/D exchange.

**E<sub>CO2</sub> Product Dynamics.** The DO<sup>-</sup> product observed from the HO<sup>-</sup> + CD<sub>3</sub>OOH reaction strongly suggests H/D scrambling that involves HOD and HO<sup>-</sup> in the complex prior to dissociation (eqs 11 and 12). The kinetic analysis shows the ratio of HO<sup>-</sup> to DO<sup>-</sup> from this complex to be roughly 9:1 (Scheme 3). The experimental results suggest encounters of hydroxide and water species during the complex lifetime, although the scrambling is incomplete far below the statistical partitioning limit of [HO<sup>-</sup>]/[DO<sup>-</sup>] = 2:1. A similar H/D scrambling involving hydrogen fluoride and hydroxide anion has been suggested from observation of DO<sup>-</sup> in the E<sub>CO2</sub> reaction of F<sup>-</sup> + CD<sub>3</sub>OOH,<sup>5</sup> that is, [DF···CD<sub>2</sub>O···HO<sup>-</sup>] ⇌ [HF···CD<sub>2</sub>O···DO<sup>-</sup>] yielding HO<sup>-</sup> and DO<sup>-</sup> with a ratio of ~16:1.<sup>52</sup> In the fluoride case, a larger fraction of hydrogen fluoride–hydroxide anion encounters would lead to regeneration of F<sup>-</sup> via exothermic proton transfer. This process could contribute to the apparent reduction in reaction efficiency to below unity, although it is difficult to quantify this effect experimentally.

Direct dynamics trajectory calculations,<sup>14</sup> however, predict that such an intracomplex interaction between HF and HO<sup>-</sup> is negligible. Instead, approximately 30% of the F<sup>-</sup> + CH<sub>3</sub>OOH encounters (55 out of 200 trajectories) result in direct back-dissociation to the reactants,<sup>14</sup> providing another very feasible explanation for the less-than-unity reaction efficiency. Although TS1 has an energy approximately 15 kcal mol<sup>-1</sup> below that of the reactants for both F<sup>-</sup> + CH<sub>3</sub>OOH and HO<sup>-</sup> + CH<sub>3</sub>OOH at CCSD(T)/aug-cc-pVDZ//B3LYP/6-31+G(d), it is possible that

a collision with a large impact parameter and orbital angular momentum results in a large rotational energy at TS1. If there is poor coupling between the orbital motion and the internal degrees of freedom for the complex, the effective potential energy increases at TS1 and reduction of the E<sub>CO2</sub> reaction efficiency may result. This mechanism has been discussed to explain the less-than-unity efficiency in the S<sub>N</sub>2 reaction of F<sup>-</sup> + CH<sub>3</sub>Cl,<sup>53,54</sup> for which the transition state energy is about 12 kcal mol<sup>-1</sup> below the reactants.

Intriguingly, there is little indication that the leaving hydroxide anion and formaldehyde interact within the product complex. Consider the labeled reaction



The deprotonated diol anion CD<sub>2</sub>(OH)O<sup>-</sup> can form from nucleophilic condensation of hydroxide and formaldehyde (eq 24), and its formation is very exothermic (Figure 3). Termolecular association between hydroxide and formaldehyde has been measured to be very rapid, forming the diol anion.<sup>36</sup> Nonetheless, the expected CD<sub>2</sub>(OH)O<sup>-</sup> anion (*m/z* 49) was not observed from HO<sup>-</sup> + CD<sub>3</sub>OOH, nor previously from the F<sup>-</sup> + CD<sub>3</sub>OOH reaction.<sup>5</sup> The diol anion could alternatively lose dihydrogen within the complex to yield the formate anion (eq 25), a major species observed in metastable and collision-induced decompositions of CH<sub>3</sub>OO<sup>-</sup> via the intermediacy of the diol species.<sup>55</sup> On the basis of the structure, energy, and IRC calculations at the B3LYP/6-311++G\*\* level of theory,<sup>55</sup> an isolated CD<sub>2</sub>(OH)O<sup>-</sup> anion will 1,2-eliminate HD to yield DCO<sub>2</sub><sup>-</sup> with a barrier height and reaction enthalpy of about 26 and -23 kcal mol<sup>-1</sup>, respectively.<sup>55</sup> The DCO<sub>2</sub><sup>-</sup> anion was observed but with only a very minor yield (<1%) from the reaction of HO<sup>-</sup> with CD<sub>3</sub>OOH. Reexamination of the F<sup>-</sup> + CD<sub>3</sub>OOH results<sup>5</sup> also reveals negligible formation of DCO<sub>2</sub><sup>-</sup> (<0.5%).

Back-dissociation of [HOD···CD<sub>2</sub>(OH)O<sup>-</sup>]<sup>\*</sup> → [HOD···CD<sub>2</sub>O···HO<sup>-</sup>] may be the only other possibility for the fate of the deprotonated diol, if it is ever formed within the complex. Isolated CH<sub>2</sub>(OH)O<sup>-</sup> can dissociate to CH<sub>2</sub>O and HO<sup>-</sup> with no exit barrier ( $\Delta_{\text{rxn}}H_{298} \approx 32$  kcal mol<sup>-1</sup>), in good competition with the H<sub>2</sub> elimination channel, which has the lower but tight activation barrier.<sup>55</sup> In fact, in both the metastable and high-energy collision-induced dissociations of CH<sub>3</sub>OO<sup>-</sup>, the deprotonated diol intermediate yields comparable amounts of HO<sup>-</sup> and HCO<sub>2</sub><sup>-</sup>.<sup>55</sup> This suggests that the formation and back-dissociation of the diol anion is a minor process when the HCO<sub>2</sub><sup>-</sup> yield is also small. There are caveats to this proposition, however. In the low-energy collision-induced dissociation of CH<sub>3</sub>OO<sup>-</sup>, the hydroxide anion was the major product, whereas formation of the formate was extremely minor.<sup>42</sup>

In view of the varying results on diol decomposition, which are both interesting and puzzling, it is unlikely that the methyl hydroperoxide results can be discussed based solely on the energetics when the product dynamics display non-statistical behavior. Theoretical studies will greatly aid in revealing these processes. For the E<sub>CO2</sub> channel of the F<sup>-</sup> + CH<sub>3</sub>OOH reaction, the direct dynamics calculations<sup>14</sup> indicate that the hydroxide anion directly leaves the [HF···CH<sub>2</sub>O···HO<sup>-</sup>] complex while avoiding the deep potential well minimum to form the diol complex, which is the IRC product following TS1. Since the HO<sup>-</sup> + CH<sub>3</sub>OOH system has a very similar potential energy feature up to TS1 and is even more steeply downhill energetically



cally after TS1 towards the products, it is very likely that the product dynamics are also direct.

The larger  $C_2H_5OOH + HO^-$  system displays more statistical behavior, i.e., a substantial interaction between  $HO^-$  and  $CH_3CHO$  within the product complex to produce the acetaldehyde enolate anion (eq 18). The potential energy diagram (Figure 4) indicates that the formation of deprotonated diol  $CH_3CH(OH)O^-$  is even more exothermic. There is no experimental evidence, however, for the intermediacy of the  $[M-H]^-$  diol anion. The observed  $[M-H]^-$  product exhibits reactivity essentially due to the  $C_2H_5OO^-$  anion from proton transfer. Energetically,<sup>42</sup> the diol anion could also lose dihydrogen to yield the acetate anion (*m/z* 59). No such species was observed from the  $C_2H_5OOH + HO^-$  reaction within detection limits. The exothermic irreversible transformation within the complex, i.e., from acetaldehyde (eq 17) to the enolate anion (eq 18), obviously predominates over the diol anion formation. In any case, for the ethyl reaction, the nascent  $HO^-$  interacts strongly with the carbonyl within the product complex. The differential behaviors of  $HO^-$  strongly suggest that the product dynamics switch from direct to more statistical in going from the methyl to ethyl hydroperoxides, potentially reflecting different degrees of intramolecular vibrational redistribution (IVR) during complex dissociation.<sup>46</sup> Effects of size and complexity on the dynamics are being systematically studied for a variety of peroxides and base anions.

## Conclusions

Reactions of  $HO^-$  with several alkyl hydroperoxides were studied in the gas phase to shed light on the  $E_{CO2}$  reactivity and dynamics of potential biochemical importance. The intrinsic efficiency for the reaction of methyl hydroperoxide with  $HO^-$  is determined to be > 80% (overall) and > 50% ( $E_{CO2}$  channel), with the  $E_{CO2}$  reaction predominating over the exothermic proton transfer channel. The  $E_{CO2}$  reactivity could approach unit efficiency if the competing proton transfer channel were not available. Ethyl hydroperoxide reacts with  $HO^-$  via  $E_{CO2}$  and proton transfer pathways plus an additional E1cb channel. *tert*-Butyl hydroperoxide has a reactivity similar to ethyl hydroperoxide except for the lack of the  $E_{CO2}$  channel. Calculated potential energy diagrams are very similar around the key  $E_{CO2}$  transition states for the reactions of  $HO^- + CH_3OOH$  and  $HO^- + C_2H_5OOH$  as well as for  $F^- + CH_3OOH$ , consistent with the high  $E_{CO2}$  efficiencies observed. The  $E_{CO2}$  transition state for  $HO^- + CH_3OOH$  is even closer to the reactants than is the transition state for  $F^- + CH_3OOH$  to the reactants. As expected, the primary deuterium KIE is very small for  $HO^-$  reacting with  $CH_3OOH$  versus  $CD_3OOH$ .

Following the  $E_{CO2}$  transition state, the potential energy curves show steep descent towards the products. Little evidence is found for the formation of a deprotonated diol intermediate within the product complex  $[H_2O \cdots CH_2O \cdots HO^-]$ , suggesting that the nascent hydroxide species leaves the complex with a negligible interaction with formaldehyde. The deep potential energy minimum for diol anion formation appears to be avoided, a non-IRC dynamics analogous to those predicted theoretically for the  $S_N2$  reaction<sup>13</sup> of  $HO^- + CH_3F$  and the  $E_{CO2}$  reaction<sup>14</sup> of  $F^- + CH_3OOH$ . Besides the negligible diol anion formation, a proton-exchange interaction is suggested between the hydroxide and water species within the complex. The larger ethyl hydroperoxide system displays more statistical behavior so that the hydroxide anion interacts strongly with acetaldehyde in the product complex  $[H_2O \cdots CH_3CHO \cdots HO^-]$ , forming  $^-CH_2CHO$  as a major product. In addition to experiments and

energetics discussions, direct dynamics trajectory studies will be very helpful and insightful to probe the dynamical aspects of these  $E_{CO2}$  reactions.

**Acknowledgment.** S.K. and V.M.B. were supported by the National Science Foundation (CHE-0647088), S.J.B. was supported by the Australian Research Council (DP0452849), and G.B.E. was supported by the United States Department of Energy (DE-FG02-87ER13695) and the National Science Foundation (CHE-9813659). S.J.B. also acknowledges the Australian Partnership for Advanced Computing (ANU, Canberra) for a generous allocation of supercomputer time. The authors thank Professor William L. Hase for helpful discussions as well as providing unpublished data. Supplementary experiments on diethyl ether and formic acid by Ms. Nicole Eyet are also appreciated.

**Supporting Information Available:** Geometries, electronic energies, zero-point energies, and imaginary frequencies used for Figures 2 and 4. This material is available free of charge via the Internet at <http://pubs.acs.org>.

## References and Notes

- (1) Kornblum, N.; DeLaMare, H. E. *J. Am. Chem. Soc.* **1951**, *73*, 880.
- (2) Hiatt, R. In *Organic Peroxides*; Swern, D., Ed.; Wiley-Interscience: New York, 1971; Vol. 2, p 1 and references therein.
- (3) King, G. K.; Maricq, M.; Bierbaum, V. M.; DePuy, C. H. *J. Am. Chem. Soc.* **1981**, *103*, 7133.
- (4) Lum, R. C.; Grabowski, J. J. *J. Am. Chem. Soc.* **1993**, *115*, 7823.
- (5) Blanksby, S. J.; Ellison, G. B.; Bierbaum, V. M.; Kato, S. *J. Am. Chem. Soc.* **2002**, *124*, 3196.
- (6) Halliwell, B.; Gutteridge, J. M. C. *Free Radicals in Biology and Medicine*, 3rd ed.; Oxford University Press: Oxford, 1999.
- (7) Murphy, R. C.; Fiedler, J.; Hevko, J. *Chem. Rev.* **2001**, *101*, 479.
- (8) Niki, E. Peroxides in biological systems. In *Organic Peroxides*; Ando, W., Ed.; John Wiley & Sons: New York, 1992.
- (9) Burcham, P. C. *Mutagenesis* **1998**, *13*, 287.
- (10) Marnett, L. J. *Carcinogenesis* **2000**, *21*, 361.
- (11) Sies, H. *Oxidative Stress*; Academic Press: London, 1985.
- (12) Hofmann, R.; Hübner, H.; Just, G.; Krätzsch, L.; Litkowitz, A. K.; Pritzkow, W.; Rolle, W.; Wahren, M. *J. Prakt. Chem.* **1968**, *37*, 102.
- (13) Sun, L.; Song, K.; Hase, W. L. *Science* **2002**, *296*, 875.
- (14) López, J. G.; Vayner, G.; Lourderaj, U.; Addepalli, S. V.; Kato, S.; deJong, W. A.; Windus, T. L.; Hase, W. L. *J. Am. Chem. Soc.* **2007**, *129*, 9976.
- (15) Blanksby, S. J.; Bierbaum, V. M.; Ellison, G. B.; Kato, S. *Angew. Chem. Int. Ed.* **2007**, *46*, 4948.
- (16) Van Doren, J. M.; Barlow, S. E.; DePuy, C. H.; Bierbaum, V. M. *Int. J. Mass Spectrom. Ion Processes* **1987**, *81*, 85.
- (17) Bierbaum, V. M. Flow tubes. In *Encyclopedia of Mass Spectrometry: Theory and Ion Chemistry*; Gross, M. L., Caprioli, R., Eds.; Elsevier: Amsterdam, 2003; Vol. 1, pp 276.
- (18) Blanksby, S. J.; Ramond, T. M.; Davico, G. E.; Nimlos, M. R.; Kato, S.; Bierbaum, V. M.; Lineberger, W. C.; Ellison, G. B.; Okumura, M. *J. Am. Chem. Soc.* **2001**, *123*, 9585.
- (19) DePuy, C. H.; Bierbaum, V. M. *J. Am. Chem. Soc.* **1981**, *103*, 5034.
- (20) de Koning, L. J.; Nibbering, N. M. M. *J. Am. Chem. Soc.* **1987**, *109*, 1715.
- (21) Spänel, P.; Pavlik, M.; Smith, D. *Int. J. Mass Spectrom. Ion Processes* **1995**, *145*, 177.
- (22) Baschky, M.C.; Kass, S. R. *Int. J. Mass Spectrom.* **2000**, *195/196*, 411.
- (23) Becke, A. D. *J. Chem. Phys.* **1993**, *98*, 5648.
- (24) Lee, C.; Yang, W.; Parr, R. G. *Phys. Rev. B* **1988**, *37*, 785.
- (25) Frisch, M. J.; Trucks, G. W.; Schlegel, H. B.; Scuseria, G. E.; Robb, M. A.; Cheeseman, J. R.; Montgomery, J. A., Jr.; Vreven, T.; Kudin, K. N.; Burant, J. C.; Millam, J. M.; Iyengar, S. S.; Tomasi, J.; Barone, V.; Mennucci, B.; Cossi, M.; Scalmani, G.; Rega, N.; Petersson, G. A.; Nakatsuji, H.; Hada, M.; Ehara, M.; Toyota, K.; Fukuda, R.; Hasegawa, J.; Ishida, M.; Nakajima, T.; Honda, Y.; Kitao, O.; Nakai, H.; Klene, M.; Li, X.; Knox, J. E.; Hratchian, H. P.; Cross, J. B.; Adamo, C.; Jaramillo, J.; Gomperts, R.; Stratmann, R. E.; Yazyev, O.; Austin, A. J.; Cammi, R.; Pomelli, C.; Ochterski, J. W.; Ayala, P. Y.; Morokuma, K.; Voth, G. A.; Salvador, P.; Dannenberg, J. J.; Zakrzewski, V. G.; Dapprich, S.; Daniels, A. D.; Strain, M. C.; Farkas, O.; Malick, D. K.; Rabuck, A. D.; Raghavachari, K.; Foresman, J. B.; Ortiz, J. V.; Cui, Q.; Baboul, A. G.;

Clifford, S.; Cioslowski, J.; Stefanov, B. B.; Liu, v G.; Liashenko, A.; Piskorz, P.; Komaromi, I.; Martin, R. L.; Fox, D. J.; Keith, T.; Al-Laham, M. A.; Peng, C. Y.; Nanayakkara, A.; Challacombe, M.; Gill, P. M. W.; Johnson, B.; Chen, W.; Wong, M. W.; Gonzalez, C.; Pople, J. A. *Gaussian 03*, revision B.05; Gaussian, Inc.: Pittsburgh, PA, 2003.

- (26) Scott, A. P.; Radom, L. *J. Phys. Chem.* **1996**, *100*, 16502.  
(27) Gonzalez, C.; Schlegel, H. B. *J. Chem. Phys.* **1989**, *90*, 2154.  
(28) Gonzalez, C.; Schlegel, H. B. *J. Phys. Chem.* **1990**, *94*, 5523.  
(29) Schaftenaar, G.; Noordik, J. H. *J. Comput.-Aided Mol. Design* **2000**, *14*, 123.  
(30) Bartlett, R. J. *J. Phys. Chem.* **1989**, *93*, 1697.  
(31) Dunning, T. H., Jr. *J. Chem. Phys.* **1989**, *90*, 1007.  
(32) Su, T.; Chesnavich, W. J. *J. Chem. Phys.* **1982**, *76*, 5183.  
(33) Miller, K. J.; Savchik, J. A. *J. Am. Chem. Soc.* **1979**, *101*, 7206.  
(34) Unless otherwise specified, all thermochemical values are derived from Linstrom, P. J., Mallard, W. G., Eds. *NIST Chemistry WebBook: NIST Standard Reference Database Number 69*, National Institute of Standards and Technology: Gaithersburg, MD, 2005 (<http://webbook.nist.gov>).  
(35) Identity of the corresponding HCO<sub>2</sub><sup>-</sup> species is ambiguous from the CH<sub>3</sub>OOH reaction because of the mass overlap with the residual C<sub>2</sub>H<sub>5</sub>O<sup>-</sup> anion.  
(36) Tanner, S. D.; Mackay, G. I.; Bohme, D. K. *Can. J. Chem.* **1981**, *59*, 1615.  
(37) A minor amount of deprotonated acetone (*m/z* 57) is also observed (~ 1%). The origin is unknown; however, it may arise from an acetone impurity either in the reagent or formed during the gas handling.  
(38) Scheme 4 predicts the ratio of [formed H<sup>16</sup>O<sup>-</sup>]/[depleted H<sup>18</sup>O<sup>-</sup>] to be 0.60. The observed value of 0.40 (with error bars of ± 0.02 accounting only for the ion counting statistics) is somewhat smaller, but not unreasonable if one takes into account a systematic bias due to overall mass discrimination against H<sup>16</sup>O<sup>-</sup> relative to H<sup>18</sup>O<sup>-</sup> under experimental conditions. Small amounts of unknown reactive impurities such as diethylether would also contribute to H<sup>18</sup>O<sup>-</sup> depletion without production of H<sup>16</sup>O<sup>-</sup>.  
(39) DePuy, C. H.; Gronert, S.; Mullin, A.; Bierbaum, V. M. *J. Am. Chem. Soc.* **1990**, *112*, 8650.  
(40) In search of a mechanism for alkoxide production, we attempted to locate transition states for S<sub>N</sub>2 reactions at oxygen with no success so far. Alternatively, the alkoxide anions may possibly be formed from HO<sup>-</sup>

deprotonation of ROH impurities, which could be formed in situ under experimental conditions via heterogeneous decompositions of the alkyl hydroperoxides in the gas transfer line and/or the flow tube, as observed for HOOH (ref 41).

- (41) Ramond, T. M.; Blanksby, S. J.; Kato, S.; Bierbaum, V. M.; Davico, G. E.; Schwartz, R. L.; Lineberger, W. C.; Ellison, G. B. *J. Phys. Chem. A* **2002**, *106*, 9641.  
(42) Blanksby, S. J.; Kato, S.; Bierbaum, V. M.; Ellison, G. B. *Aust. J. Chem.* **2003**, *56*, 459.  
(43) Ikezoe, Y.; Matsuoka, S.; Takebe, M.; Viggiano, A. *Gas Phase Ion-Molecule Reaction Rate Constants Through 1986*; Maruzen: Tokyo, 1987.  
(44) Zhang, X.; Bierbaum, V. M.; Ellison, G. B.; Kato, S. *J. Chem. Phys.* **2004**, *120*, 3531.  
(45) Zhang, X.; Kato, S.; Bierbaum, V. M.; Nimlos, M. R.; Ellison, G. B. *J. Phys. Chem. A* **2004**, *108*, 9733.  
(46) Baer, T.; Hase, W. L. *Unimolecular Reaction Dynamics*; Oxford University Press: New York, 1996.  
(47) Robinson, P. J.; Holbrook, K. A. *Unimolecular Reactions*; Wiley: New York, 1972.  
(48) Tyblewski, M.; Meyer, R.; Bauder, A. *8th Colloquium on High Resolution Molecular Spectroscopy*, Tours, France, 1983; cited in Haas et al. (ref 49).  
(49) Haas, B.; Oberhammer, H. *J. Am. Chem. Soc.* **1984**, *106*, 6146.  
(50) Bierbaum, V. M.; Filley, J.; DePuy, C. H.; Jarrold, M. F.; Bowers, M. T. *J. Am. Chem. Soc.* **1985**, *107*, 2818.  
(51) Eyet, N.; Villano, S. M.; Kato, S.; Bierbaum, V. M. *J. Am. Soc. Mass Spectrom.* **2007**, *18*, 1046.  
(52) In the earlier work, the ratio of HO<sup>-</sup> to DO<sup>-</sup> was reported to be ~6:1 (ref 5). The revised ratio comes from full analysis to extract the primary branching ratio, which corresponds to the relative product yields of HO<sup>-</sup> (82%) and DO<sup>-</sup> (5%).  
(53) Su, T.; Wang, H.; Hase, W. L. *J. Phys. Chem. A* **1998**, *102*, 9819.  
(54) Wang, H.; Hase, W. L. *J. Am. Chem. Soc.* **1997**, *119*, 3093.  
(55) Schalley, C. A.; Schröder, D.; Schwarz, H.; Möbus, K.; Boche, G. *Chem. Ber.* **1997**, *130*, 1085.

JP800702Z